Transparent Epidermal Antenna for Unobtrusive Human-Centric Internet of Things Applications

Roy B. V. B. Simorangkir, *Member, IEEE*, Dinesh R. Gawade, *Member, IEEE*, Tim Hannon, *Member, IEEE*, Paul Donovan, *Member, IEEE*, Sanjeev Kumar, *Member, IEEE*, Nadeem Rather, *Student Member, IEEE*, Gholamhosein Moloudian, *Member, IEEE*, Brendan O'Flynn, *Senior Member, IEEE*, and John L. Buckley, *Member, IEEE*

***Abstract*—The concept of optical transparency in antennas for epidermal electronics is demonstrated in this work as a means of improving the long-term comfort-of-wear level and possibly opening up a wider range of applications. In contrast to previous attempts, the epidermal antenna transparency is achieved by employing dielectric and conductive materials that are both transparent and flexible (i.e., polydimethylsiloxane transparent conductive textile composite) via a nonclean room procedure that is relatively simpler and less expensive. To demonstrate the concept, a modified rectangular loop epidermal antenna for an arm-worn wireless sensing system operating at 868-MHz ultra high-frequency (UHF) band is designed. Through a systematic numerical investigation, an interesting radiation response of the loop epidermal antenna as the result of two opposing mechanisms of radiation and loss is revealed, which dictates a specific design guideline for the loop when attached to the body compared to that in free space. Two antenna prototypes were fabricated with the developed transparent composite and its nontransparent counterpart. Then, comprehensive characterizations comparing both epidermal antenna prototypes were carried out, including antenna return loss and far-field tests on a human forearm phantom, and indoor wireless connectivity tests using a human test subject. By showing similar performance between the two prototypes, the study provides a convincing demonstration of the applicability of the developed transparent composite for the class of epidermal antenna and the capability of a transparent antenna to enable wireless connectivity in the context of epidermal electronics.**

***Index Terms*—Conductive textile, epidermal antenna, flexible antenna, Internet of Things (IoT), polydimethylsiloxane (PDMS), transparent antenna, unobtrusive, wearable antenna.**

Manuscript received 20 March 2023; revised 31 May 2023; accepted 18 June 2023. Date of publication 23 June 2023; date of current version 25 December 2023. This work was supported in part by the Irish Research Council under Award GOIPD/2022/390; in part by the Enterprise Ireland funded HOLISTICS DTIF Project under Grant EIDT20180291-A; in part by the Science Foundation Ireland (SFI) through the SFI Centre VistaMilk under Grant SFI 16/RC/3835, through the Connect Centre for Future Networks and Communications under Grant 13/RC/2077, and through the Insight Centre for Data Analytics under Grant SFI/12/RC/2289; and in part by the European Regional Development Fund. *(Corresponding author: Roy B. V. B. Simorangkir.)*

This work involved human subjects or animals in its research. Approval of all ethical and experimental procedures and protocols was granted by the University College Cork Clinical Research Ethics Committee (UCC CREC) under Application No. ECM 4 (ss).

Roy B. V. B. Simorangkir, Dinesh R. Gawade, Sanjeev Kumar, Nadeem Rather, Gholamhosein Moloudian, Brendan O'Flynn, and John L. Buckley are with the Wireless Sensor Network Group, Tyndall National Institute, University College Cork, Cork, T12R5CP Ireland (e-mail: roy.simorangkir@ieee.org).

Tim Hannon and Paul Donovan are with Sanmina Corporation, Huntsville, AL 35803 USA.

Digital Object Identifier 10.1109/JIOT.2023.3288994

I. Introduction

THE PHRASE epidermal electronics refers to an electronic system in which all functionality and associated active and passive components, ranging from electrodes, sensors, electronics, communication, and power supply modules, are embodied in a skin-compatible ultrathin form factor. The concept was introduced in 2011 [1], with the goal of revolutionizing human physiological sensing technologies, which have historically relied on wired interconnections between skin-attached sensors/electrodes and external entities containing signal conditioning units, data storages, communication modules, and power supplies. The notion of epidermal electronics is to create a device that features as many characteristics of human skin as possible (e.g., ultra thinness, flexibility, stretchability, self-healing, and air/water permeability, to mention a few) while still fulfilling certain functions. With such distinct qualities, epidermal electronics have opened up a plethora of new possibilities, notably in the fields of real time and truly noninvasive human physiological monitoring and human-machine interface, addressing problems that traditional wearable electronics cannot [1], [2], [3].

Epidermal antenna is one of the key components of the radio frequency (RF) front end of epidermal electronics. Its purpose is to enable wireless communication capability and/or self-powering of the epidermal electronics [2], [4]. As the name pertains, epidermal antenna refers to a single-layer skin-attached antenna separated from the human epidermis by a submillimeter-thick flexible membrane [5], [6]. In the recent few decades, there has been a lot of research interest in this area, especially with the rapid growth of the wearables research and industry [7], [8]. A variety of antenna topologies, including coils/loops [5], [9], [10], [11], [12], [13], [14], dipoles [15], [16], [17], monopoles [18], slots [19], [20], and even arrays [21], have been explored in conjunction with the implementation of different materials as well as manufacturing techniques. These explorations have resulted in successful demonstrations of various applications in the context of Internet of Things (IoT) for human-centric systems, such as finger augmentation devices for pressure [16] and dielectric sensing [15], batteryless breathing [13], [17], temperature [14], and sweat [9], [22] monitoring systems, biotelemetry [5], and smart indoor human tracking [23], to name a few.

In the context of electronics mounted on human skin, producing an epidermal antenna with the highest comfort-of-wear level is just as critical as developing a high-performance antenna. Being typically the most space-occupying component, the less disruption created by the antenna's physical existence in the users' daily activities, the more likely people are to wear the epidermal device [24]. One key engineering approach to achieving comfort-of-wear is to impart skin conformability to the epidermal antenna. Adding to that, if both of the antenna substrate and radiator can be made optically transparent, it will enhance further the wearers' comfort for long-term usage and aesthetic appearance, thus increasing the proliferation of the epidermal electronics and even renders vast areas of applications. In the case of smart wound dressing [25], for instance, the transparent attribute of the antenna and integrated electronics would enable clinicians to obtain real-time visualization and a more accurate evaluation of the wound healing progress without having to remove the dressing. For wireless sensing and monitoring devices equipped on the body of mental health patients and elderly [26], [27], visually imperceptible wearable devices will improve the reliability of long-term health monitoring and surveillance. Despite the benefits, the majority of the aforementioned studies on epidermal antenna have not demonstrated the concept of transparency in its entirety. For instance, in [13], [14], [15], [16], [17], [22], and [28], while the works employ transparent materials as the antenna substrate, the conductor is still realized with opaque materials. This scarcity may be attributable to the challenges of fabricating optically transparent flexible antennas [29]. In particular, finding conductive materials with an optimal balance of conductivity, optical transparency, and mechanical robustness is notoriously difficult. In addition, the fabrication process is often costly and entails a series of complex procedures.

We recently proposed a new method for realizing transparent flexible antennas in [30] through layer-by-layer assembly of polydimethylsiloxane (PDMS) and patterned transparent conductive textile. The demonstrated concept is comparatively simpler and less expensive than other popular approaches based on transparent conductive oxides, transparent conductive polymers, silver nanowires, and 2-D materials [such as graphene, MXene, and molybdenum disulfide (MoS2)], which typically involve complex processes (e.g., physical/chemical vapor deposition, RF sputtering, lithography, electrospinning, and spray pyrolysis, to name a few) [30]. The resultant antennas displayed noteworthy qualities of high transparency (i.e., $>$70% optical transmittance), flexibility, durability against humidity and deformation, while concurrently showing a good reproducible RF performance.

In this work, to further advance the field of epidermal electronics, we investigate for the first time the potential of implementing our proposed concept, PDMS-transparent conductive textile composite, for the realization of optically transparent epidermal antennas. To do this, we design, fabricate, and characterize a modified rectangular loop antenna operating at 868-MHz ultra high-frequency (UHF) band made of the aforementioned composite material. First, we present a systematic numerical examination of the antenna response as a function of different design parameters when attached on a phantom representing human arm tissue. By revealing an interesting response of a loop antenna in a close proximity to a human body, this study offers insight and general guidelines toward producing an epidermal antenna with the optimum performance. A comprehensive evaluation of the antenna performance was conducted, including reflection coefficient, far-field, wireless communication, and specific absorption rate (SAR) numerical tests. The wireless communication tests were carried out in an indoor long-range wide area network (LoRaWAN) testbed, which involved a number of LoRa gateways and a battery-powered wireless module with the developed epidermal antenna connected and worn on the forearm of a human subject. The results show a good performance in terms of antenna input impedance matching, radiation and hence wireless connectivity, as well as RF exposure, demonstrating the applicability of the developed composite for the class of epidermal antenna.

In this study, we also constructed an opaque prototype counterpart of the developed design out of PDMS and nontransparent conductive textile composite [31]. For the first time, we present a thorough examination comparing the performance of opaque and transparent epidermal antennas, numerically and experimentally. Despite the variation in conductive textile quality, the results show no appreciable difference particularly in the radiation performance and hence the wireless link quality, corroborating the earlier research by [6]. This discovery is significant, particularly in the context of epidermal antenna development, as it confirms that during the construction of an epidermal antenna, the designer may focus their efforts on other goals than perfecting the conductor quality to boost the radiation, if the σ is larger than 10^4 S/m [6]. More importantly, the findings provide a compelling demonstration of the capability of the transparent antenna for enabling wireless functionality of epidermal electronics in the context of human-centric IoT.

II. Materials

The fabrication of the proposed transparent epidermal antenna employs Less EMF VeilShield and Dow Corning Sylgard 184 for the antenna conductive and nonconductive parts, respectively. On the other hand, for the nontransparent counterpart, Less EMF Nickel(Ni)-Copper(Cu)-coated ripstop is used. VeilShield is a commercial woven conductive textile made of monofilament polyester threads that are coated with Cu and Zinc (Zn)-blackened Ni. According to the supplier's data sheet, the textile has a thickness of 57 μm with a sheet resistance of 0.1 $\Omega/\square$. The warp and weft threads interlace in one-to-one ratio at approximately 0.17-mm distance, resulting in a see-through textile with 132/inch mesh. Using an Agilent Carry 5000 UV-vis-NIR spectrophotometer, we assessed that this particular textile has an optical transmittance of approximately 72% in the visible light spectrum between 350 and 750 nm. Unlike VeilShield, the Ni-Cu-coated ripstop is a commercial woven textile constructed of multifilament threads covered with metal. The distance between the warp and weft groups intertwining in a one-to-one ratio is less than 0.04 mm, resulting in a good resemblance to a solid metallic plate. The

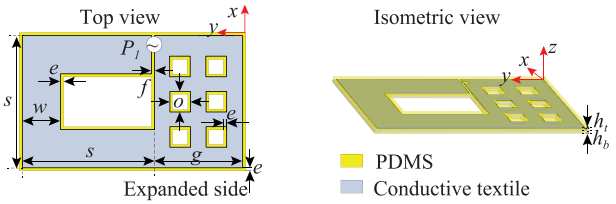

Fig. 1. Layout of the proposed epidermal antenna. Dimensions (all in millimeters): $s = 45$ mm, $g = 30$ mm, $w = 13$ mm, $o = 7$ mm, $f = 1$ mm, $e = h_t = h_b = 0.5$ mm.

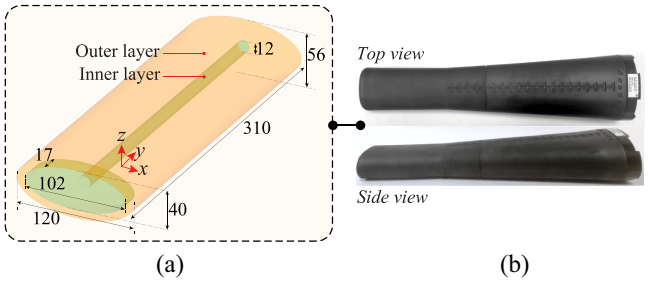

Fig. 2. (a) Simplified simulation model of SHO-GFPC-V1 forearm phantom (all dimensions are in millimeters). (b) Actual SHO-GFPC-V1 forearm phantom from SPEAG.

supplier's data sheet describes this textile as having a thickness of 80 μm and a sheet resistance of 0.03 $\Omega/\square$. The coating material of both textiles contain Ni, a common allergen that can induce contact dermatitis [32]. However, this problem is mitigated by the fact that in this work the textile is completely encapsulated in PDMS, which is biocompatible. Sylgard 184, a silicone elastomer supplied as a two-component liquid kit, was used to prepare the PDMS solution by mixing the base and the curing agent of the kit in a ten-to-one weight ratio. PDMS has an approximate relative permittivity (ε_r) of 2.8 and tanδ of 0.015 at 868 MHz as determined by experiments conducted with an Agilent 85070E Dielectric Kit. Noting that PDMS is a suitable material for epidermal electronics due to its unique properties, such as high flexibility/stretchability, transparency, water- and heat-resistance, and chemical stability [31].

III. Proposed Antenna

A. Topology

The proposed epidermal antenna is based on a rectangular loop antenna, with one of its sides expanded, resulting in an unbalanced loop structure (see Fig. 1). This transformation is intended to mitigate common mode currents that typically flow when a balanced antenna or an antenna with a small ground plane is fed with an unbalanced feeding line (e.g., the coaxial cable used in the antenna characterizations described in the following sections) [33], [34]. These currents flowing in the outer conductor of the coaxial cable cause the cable to become an integral part of the antenna, which can lead to measurement errors. The proposed antenna radiator made of the conductive textile is fully encapsulated by PDMS. A number of square-shaped holes are punched into the expanded side to facilitate air and water permeability, hence alleviating the nonbreathability issue of PDMS. Simulations revealed that the holes have no significant influence on the input impedance and radiation performance of the antenna (approximately 0.1-dB gain difference between antennas with and without holes). The antenna is envisaged for an arm-worn wireless sensing application operating at the European LoRaWAN frequency band, i.e., 863–870 MHz. LoRaWAN was chosen as the radio technology because of its attractive features of long-range communication with cost-effective infrastructure, high-network reliability (packet delivery ratio (PDR) > 0.995), and low-power consumption (< 105 mW) [35].

It should be noted that when a loop antenna is electrically large, the distinction between its magnetic and electric fields is less obvious. In our case, denoting the effective permittivity sensed by the antenna when placed on a phantom as $\varepsilon_{\text{eff}} = (\varepsilon_{\text{phantom}}+1)/2$ [6], [36], the aperture/perimeter of the loop ($4s$) is electrically large, i.e., $2.05\lambda_{\text{eff}}$. Consequently, in terms of gain and efficiency, this loop antenna typically demonstrates no distinct advantages over its electric counterparts in operation near the human body. Nevertheless, in contrast to other antenna structures widely used for epidermal electronics (e.g., dipole and slot antennas), a loop antenna exhibits a smaller optimal size and a more stable input impedance [6]. In addition to that, the selection of the loop topology took into account the convenience of implementation on the target part of the human body.

B. Simulation Setup

The design and optimization of the antenna were performed using full-wave electromagnetic simulators ANSYS HFSS and CST Microwave Studio 2020. Given the target implementation, the simulations were done with the antenna placed directly on a forearm phantom. During the design and optimization phases, the elliptical cylinder phantom model depicted in Fig. 2(a) was used in simulations. The model is a simplified replica of the SHO-GFPC-V1 forearm phantom from SPEAG [37] shown in Fig. 2(b), which was used for the antenna characterizations described in Section V. SHO-GFPC-V1 is a commercial anthropomorphic forearm phantom developed by SPEAG in conjunction with cellular telecommunications and Internet association (CTIA) for the over-the-air (OTA) performance test plan of forearm-mounted transmitters/receivers [37], [38]. The phantom is mainly composed of silicone–carbon powder compound based on [39] that surrounds and fills a tube-supporting structure made of prepreg material. The silicone–carbon composition was optimized so that its RF dielectric properties matched those of the human forearm as identified by coaxial probe-based measurements done in [40] and [41]. Following the construction of SHO-GFPC-V1, the inner layer of the phantom model in Fig. 2(a) represents the silicone–carbon filled-tube and was modeled with ϵ_r of 30 and conductivity (σ) of 2.5 S/m. The outer layer, which was modeled with ϵ_r of 30 and σ of 0.7 S/, represents the silicone–carbon compound surrounding the tube. These electrical properties are based on the data provided by the SPEAG representatives for our target operating frequency of 868 MHz. In simulations, the nonconductive parts of the

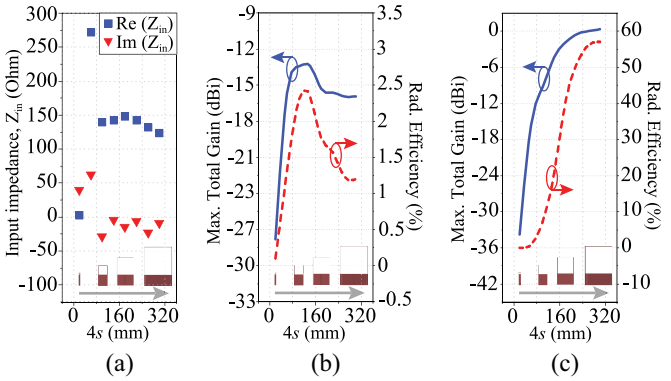

Fig. 3. Antenna performance at 868 MHz as a function of loop aperture ($4s$): (a) input impedance and (b) total gain/radiation efficiency when mounted on the phantom, and (c) total gain/radiation efficiency when the phantom was removed. When $4s$ was varied, other parameters were set as: $g = 30$ mm, $w = 1$ mm, $f = 1$ mm, $e = h_t = h_b = 0.5$ mm and the holes were removed for simplicity. The inset shows the topology of the antenna as $4s$ varies.

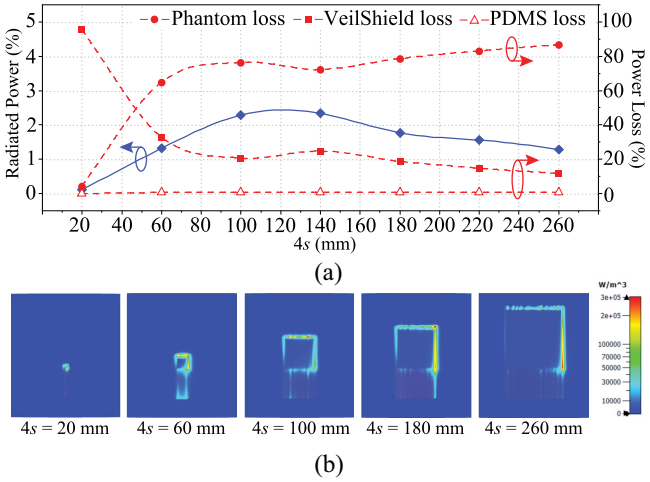

Fig. 4. (a) Antenna power analysis at 868 MHz as a function of loop aperture ($4s$). (b) Power loss density of the phantom at 868 MHz as $4s$ increases.

antenna were modeled with the measured properties of PDMS described in Section II. On the other hand, the conductive parts were modeled as a section having the thickness of the associated textile and an updated sheet resistance to account for the percolation of PDMS into the pores of the chosen textile, i.e., 0.7 Ω/□ and 0.23 Ω/□ for the transparent and nontransparent textiles, respectively [30], [31].

C. Epidermal Antenna Parametric Study

With an aim to identify the optimal configuration of the proposed transparent antenna, the antenna responses as a function of dimensions, particularly the loop aperture ($4s$), trace width (w), expanded side width (g), and bottom PDMS layer thickness (h_b), were investigated. The study was performed numerically with the antenna mounted on the phantom model specified previously. The antenna responses were recorded in terms of the antenna input impedance, total gain, and radiation efficiency. Though only the performance of the transparent version is provided in this section, the same trend was observed in the nontransparent counterpart.

Fig. 3(a) and (b) show, respectively, the antenna input impedance and total gain/radiation efficiency with varying aperture ($4s$). For a comparison, Fig. 3(c) depicts the radiation performance as a function of $4s$ when the phantom is nonexistent. As expected, the antenna input impedance fluctuates [see Fig. 3(a)] as the antenna physical dimensions and, consequently, the antenna coupling to the phantom change. Comparing Fig. 3(b) and (c), a low-radiation level is immediately noticed when the phantom is present. This is understandable for the case of a nonshielded antenna placed in a very close proximity to a human-body-emulating phantom. With the impedance matching aspect neglected, such a low radiation is primarily attributed to the significant power losses in the phantom. It is, however, more interesting to note that in the case of with phantom, the antenna radiation performance exhibits a bell-shaped trend [see Fig. 3(b)]. As $4s$ expands, initially the gain and radiation efficiency increase rather linearly, then reach a peak, before declining somewhat. Similar occurrence was also reported in [6]. Such a behavior is in contrast to the case when the loop antenna operates in free space. As can be seen in [Fig. 3(c)], the free-space antenna gain and radiation efficiency typically have a positive correlation with the antenna aperture.

To further comprehend Fig. 3(b), simulations were carried out to analyze the antenna overall power distribution at 868 MHz, and the results are presented in Fig. 4(a). As can be seen, the antenna radiated power rises as $4s$ increases upto 120 mm. On the other hand, the VeilShield loss shows a continuous drop as $4s$ grows. From these two plots, it can be deduced that the antenna radiation resistance does increase as a function of loop aperture, which is the reason for the early increase in the antenna gain and radiation efficiency depicted in Fig. 3(b) till $4s = 120$ mm. However, as the antenna aperture grows larger, the phantom loss, which appears to be very dominant, increases as the probability of reactive and radiative fields coupling to the phantom also increases [indicated by the power loss density distribution in Fig. 4(b)]. Beyond $4s = 120$ mm, the phantom loss appears to be more prominent, causing the decline in the radiated power plot, and thus the gain and radiation efficiency plots [see Fig. 3(b)].

Figs. 5 and 6 show the antenna performance with varying trace width (w) and expanded side width (g), respectively. The results indicate that unlike $4s$, the variation of w and g has an insignificant effect on the antenna radiation performance. Wider w and g yield similar radiation performance as that of the narrow case [see Figs. 5(b) and 6(b)]. On the other hand, as can be seen in Figs. 5(a) and 6(a), the antenna input resistance and reactance can be tuned by varying w and g.

Finally, the antenna performance as a function of bottom PDMS layer thickness (h_b), which essentially governs the loop-phantom distance, is shown in Fig. 7. As predicted, the distance between the antenna and phantom has a substantial impact on the antenna input impedance and radiation performance even with a small change. As the antenna is placed further away from the phantom (the thickness of the PDMS bottom encapsulation increases), the reactive fields

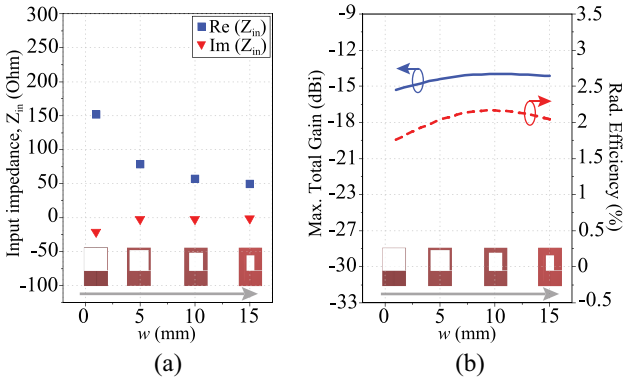

Fig. 5. Performance of the antenna on the phantom at 868 MHz as a function of trace width (w): (a) input impedance and (b) total gain/radiation efficiency. When w was varied, other parameters were set as: $s = 45$ mm, $g = 30$ mm, $f = 1$ mm, $e = h_t = h_b = 0.5$ mm and the holes were removed for simplicity. The inset shows the topology of the antenna as w varies.

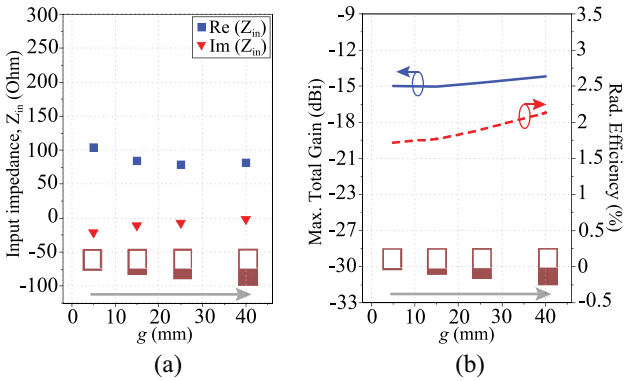

Fig. 6. Performance of the antenna on the phantom at 868 MHz as a function of expanded side width (g): (a) input impedance and (b) total gain/radiation efficiency. When g was varied, other parameters were set as: $s = 45$ mm, $w = 5$ mm, $f = 1$ mm, $e = h_t = h_b = 0.5$ mm and the holes were removed for simplicity. The inset shows the topology of the antenna as g varies.

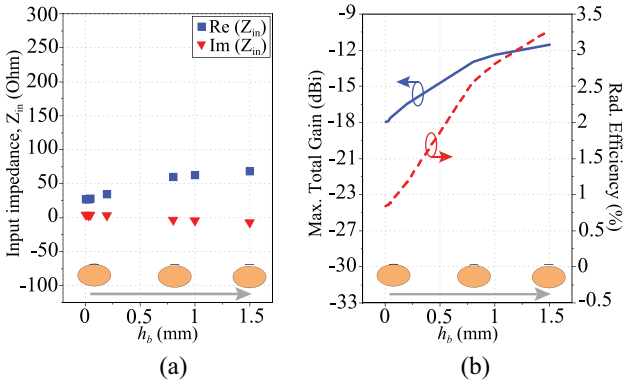

Fig. 7. Performance of the antenna on the phantom at 868 MHz as a function of bottom PDMS layer thickness (h_b): (a) input impedance and (b) total gain/radiation efficiency. When h_b was varied, other parameters were set as: $s = 45$ mm, $w = 13$ mm, $f = 1$ mm, $e = h_t = 0.5$ mm and the holes were removed for simplicity. The inset shows the topology of the antenna on the phantom as h_b varies, seen from the x-z plane.

coupling to the tissue decreases, which impacts the antenna overall impedance calculated at the feed point. Less coupling to the tissue also results in less power loss in the phantom and a larger optimal size of the antenna, which together

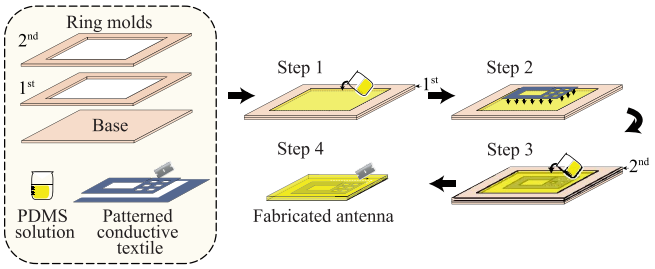

Fig. 8. Schematic illustration of the antenna fabrication process through layer-by-layer PDMS-textile assembly.

lead to a significant rise in the antenna gain and efficiency. It is important to note that, with the initial liquid state of PDMS, nearly any thicknesses can be achieved. The thickness of the PDMS encapsulation layer is then determined by a compromise between the expected electrical and mechanical properties of the resulting epidermal antenna.

The above-stated findings can then be summed up to constitute practical design guidelines for the proposed antenna. First, the aperture of the loop and the thickness of bottom PDMS layer can be employed as a key antenna radiation performance control. Second, the optimum loop aperture is the balance point between the opposing mechanisms of radiation and loss. Third, the loop width and the expanded side width can be used to tune the antenna input impedance to achieve matching. With the above in mind, the antenna was optimized, and its final dimensions are given in the caption of Fig. 1.

IV. Epidermal Antenna Fabrication

As illustrated in Fig. 8, the antenna prototypes were constructed through a layer-by-layer polymer-textile assembly process, starting from the bottom to the top encapsulation layer. Two customized ring molds each having a thickness of 0.5 mm were used to achieve the thickness of the PDMS encapsulation layers. It is important to note that with the initial liquid nature of PDMS, there is a high flexibility to further reduce the thickness of the encapsulation layer for a higher antenna mechanical compatibility with the skin. Upon degassing in a vacuum desiccator for 20 min to remove the trapped air bubbles, the PDMS solution was poured in the mold and cured in the oven at 80° C for 30 min to make the encapsulation layer. The conductive textile was patterned manually using a razor blade following the design in Fig. 1. The attachment of the textile on the cured bottom encapsulation layer was done using the uncured PDMS followed by curing in the oven at 80° C for 5 min. For the transparent textile, prior to the textile attachment, a sticky tape was adhered to the feeding point to resist the PDMS to PDMS bonding at that particular location. This was required to facilitate the attachment of a 50 Ω U.FL connector detailed below, which is needed for antenna measurement purposes.

Upon curing of the top encapsulation layer, the fabricated prototype was peeled from the mold and the excess PDMS was trimmed from the edges. The PDMS was also cut to create the holes in the middle of the loop and on the antenna expanded side. The top PDMS layer was scratched

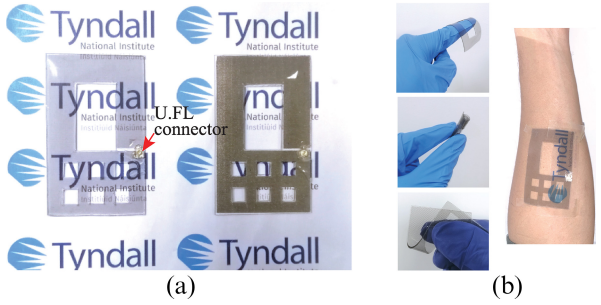

Fig. 9. (a) Transparent epidermal antenna prototype compared to its nontransparent counterpart. (b) Transparent epidermal antenna when laid on an index finger, bent and rolled by hand, and mounted on a forearm. A printed Tyndall logo is added underneath the antenna to illustrate its see-through feature.

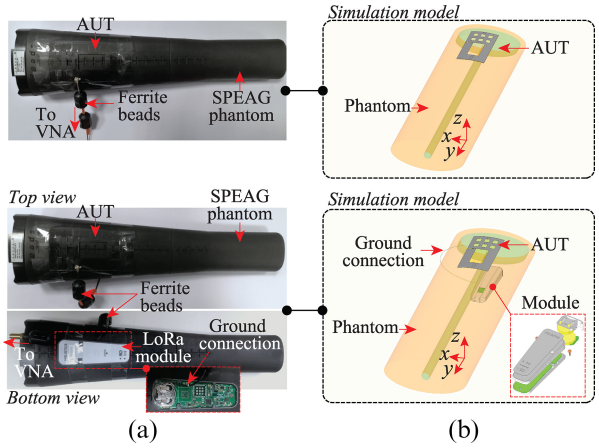

Fig. 10. Antenna setups for $|S_{11}|$ and far-field measurements: (a) without and (b) with the wireless module connected.

at the feeding point location slightly to expose the textile for the U.FL connector attachment. In the transparent prototype case, this would not have been possible without the sticky tape due to the strong integration achieved between PDMS and the transparent conductive textile. The U.FL connector was attached to the exposed textile (upon detaching the tape in the transparent case) with conductive silver epoxy (Chemtronics CircuitWorks), followed by curing in the oven at 80° C for 10 min. PDMS encapsulation (10 min oven curing time at 80° C) was applied at the connector-textile interface to strengthen the interconnection. Fig. 9 shows the photographs of the fabricated prototypes. In particular, the transparent antenna demonstrates the wearability aspects of transparency (approximately 70% measured optical transmittance) [Fig. 9(a)], high flexibility, durability, as well as air permeability [Fig. 9(b)].

V. Antenna Performance

Holistic investigations were carried out to evaluate the performance of the developed antenna prototypes, comparing the transparent and nontransparent counterparts. They included the testings of the antenna input reflection coefficient ($|S_{11}|$) and far-field characteristics, as well as indoor wireless communication tests. In addition, a numerical analysis was conducted on the impact of the antenna on the underlying human body tissue in terms of RF exposure.

A. $|S_{11}|$ Tests

Fig. 10 shows the setup for the $|S_{11}|$ measurements conducted using an MS2038C vector network analyzer (VNA) from Anritsu. Two measurement scenarios were investigated: 1) before [Fig. 10(a)] and 2) after [Fig. 10(b)] connecting the antenna to a customized LoRa module, which was developed for the purpose of wireless communication tests. In both scenarios, the antenna was mounted on the SHO-GFPC-V1 forearm phantom. The measurement setup was mimicked in the simulation as can be seen on the right side of Fig. 10. In the second scenario, the LoRa module was placed on the opposite side of the antenna to minimize the impact of the module on the antenna impedance matching. This is considering that the epidermal antenna was designed and optimized as a stand-alone component as opposed to the LoRa module-integrated antenna. To note that rather than proposing a system, the emphasis of this work is on the component level, specifically the development of antennas. In addition, the wireless module that was developed solely for testing purposes is still physically incompatible for a seamless integration with the antenna. Tape was used to attach the antenna and the module to the phantom. A U.FL-to-SMA cable was used to connect the antenna to the VNA during the measurements. Nonconductive glue was applied at the feed location to strengthen the interconnection between the U.FL connector and the cable. For the second scenario, the outer part of the U.FL-to-SMA cable was connected to the ground of the wireless module board to mimic the actual implementation during the wireless tests, i.e., the antenna and the board's ground is connected through the feed point.

In both scenarios of $|S_{11}|$ tests, we performed a quick check by touching the coaxial cable connecting the antenna (and the wireless module in the second scenario) to the VNA. We observed stable $|S_{11}|$ results, which led us to believe that any common mode currents are negligible. We conducted additional simulations using the second scenario, i.e., antenna with the wireless module. We compared the antenna radiation performance of cases with and without the cable connecting the antenna and the board [see Fig. 10(b)], which replicates the ground connection explained before. The simulated result of the case with cable revealed a peak realized gain of no more than 0.2 dB higher than the case without cable, confirming the insignificance level of currents and the consequent effect of cable. Despite these findings, we still employed ferrite beads on the coaxial cables as a precaution against the common mode currents [33], [42].

Fig. 11 shows the $|S_{11}|$ performance of both the transparent and nontransparent prototypes for the two measurement scenarios mentioned above. Both antennas exhibit a wide 10-dB return loss bandwidth of more than 1 GHz covering the target frequency 868 MHz, which is in a good agreement with the simulated results. This performance is maintained even upon the integration with the LoRa module. The changes in antenna input impedance [see Fig. 11(b)] are anticipated with the antenna and ground of the module board connected, allowing

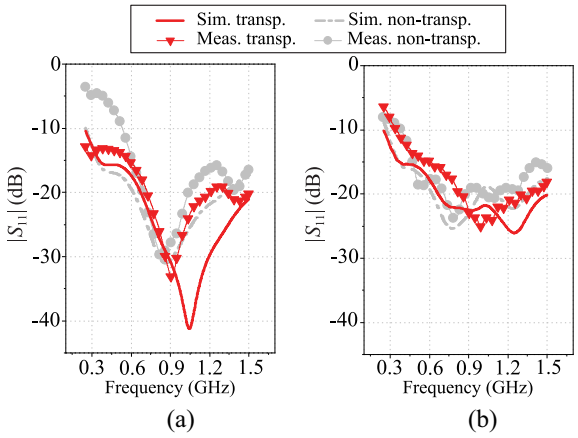

Fig. 11. Measured and simulated $|S_{11}|$ of the developed epidermal antennas, both the transparent and nontransparent counterpart, comparing the scenarios (a) without and (b) with the wireless module connected.

TABLE I
PEAK REALIZED GAINS AND RADIATION EFFICIENCIES OF THE DEVELOPED EPIDERMAL ANTENNAS AT 868 MHZ WITHOUT AND WITH THE WIRELESS MODULE CONNECTED

Scenario	Transparent		Non-transparent	
	Gain (dBi)	Eff. (%)	Gain (dBi)	Eff. (%)
Sim. without module	−14.0	1.86	−13.7	2.09
Meas. without module	−15.3	1.66	−14.5	1.94
Sim. with module	−13.0	2.06	−12.6	2.32
Meas. with module	−14.6	1.79	−13.5	2.14

slight currents to flow to the board's ground, as observed in simulation. The discrepancies between the measured and simulated results might be attributed to slight differences in the geometry of the phantom model used in the simulation versus the actual phantom, as well as manufacturing defects. The latter is more probable in the transparent antenna case due to the nature of VeilShield, which is thinner, stretchier, and more prone to fraying, particularly during manual cutting. Errors in fabrication could possibly be mitigated by employing a cutting machine that can pattern the textile with greater precision and control.

B. Far-Field Tests

The antenna radiation characterizations were performed using the AMS-8050 antenna measurement system from ETS-LINDGREN for both scenarios indicated in Fig. 10. For the same reason described previously, multiple ferrite beads were added to the feed cable. The radiation patterns of both antennas are depicted in Fig. 12 and their radiation performance is summarized in Table I, showing a good agreement between the simulated and measured results. The differences in the results might be due to the same variables identified in the $|S_{11}|$ tests. Changes in the antenna pattern, as well as a slight increase in the antenna realized gain and radiation efficiency, result directly from the minor currents flowing to the board, as described in the previous section. Typically, the radiation efficiency of antennas constructed using PDMS-conductive textiles varies by more than 10% between these two textiles

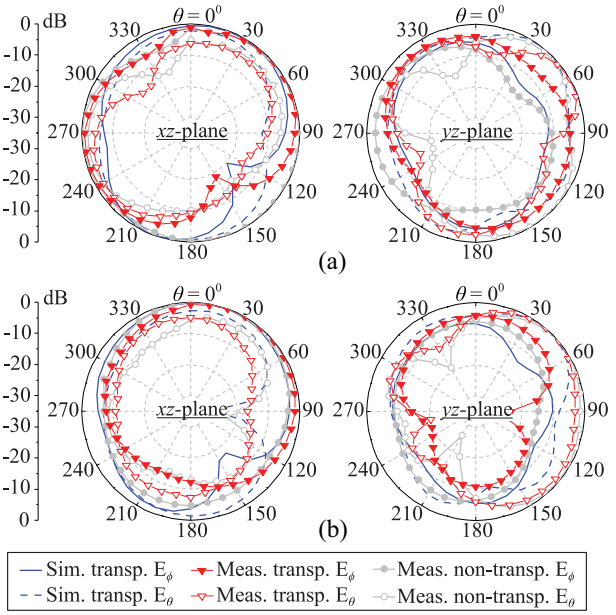

Fig. 12. Measured and simulated radiation patterns of the developed epidermal antennas, both the transparent and nontransparent counterpart, comparing the scenarios (a) without and (b) with the wireless module connected.

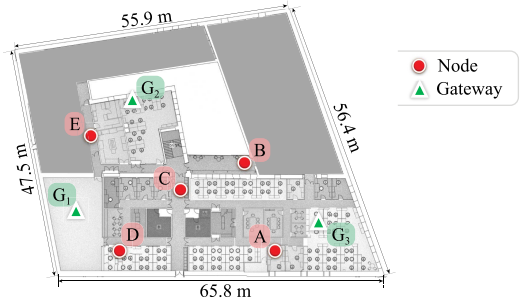

Fig. 13. LoRaWAN testbed network.

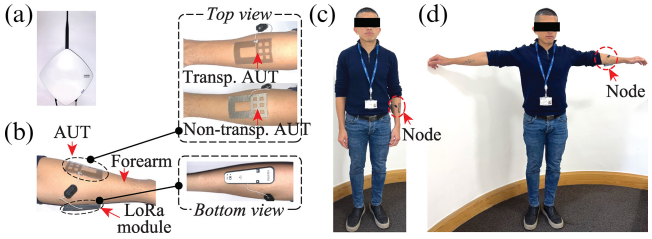

Fig. 14. (a) LoRa gateway and (b) node with transparent and nontransparent epidermal antennas. Two wireless testing scenarios: (c) test subject standing with both arms at the side of the body (scenario 1), (d) test subject standing with both arms raised (scenario 2).

(i.e., VeilShield and Ni-Cu-ripstop) [43]. However, this does not appear to be the case when the antenna is in direct contact with human tissue. Due to the dominating power losses in the human body tissue beneath, the quality of the antenna conductor appears to have a minor impact on the radiation performance.

C. Indoor Wireless Communication Tests

To demonstrate the viability of the developed epidermal antenna for IoT applications, a simple LoRaWAN testbed

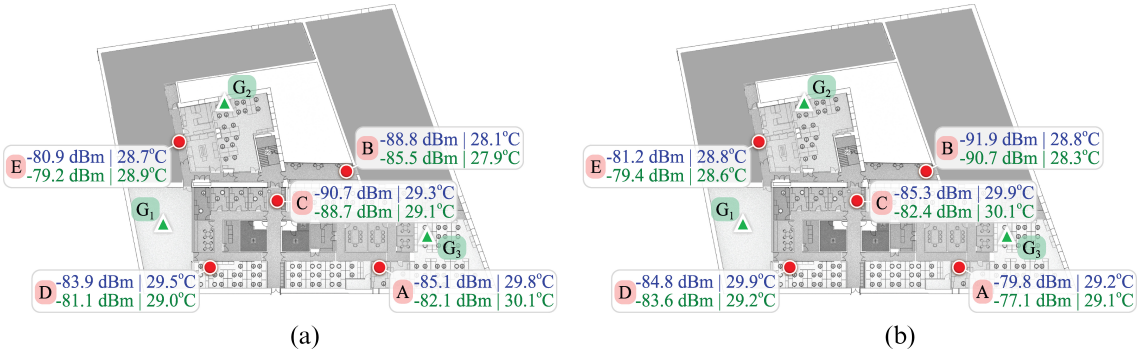

Fig. 15. Maximum average RSSI values recorded at each node location for: (a) scenario 1 and (b) scenario 2. The results with the transparent antenna are shown in blue text, whereas those with the nontransparent antenna are shown in green text.

network (Fig. 13) was deployed on the second floor of Tyndall National Institute's Block B Building. The testbed network consists of one LoRaWAN sensor node and three LoRaWAN gateways (i.e., G_1, G_2, G_3). TTN-GW-868 [Fig. 14(a)] [44], a commercial LoRaWAN gateway with an 868-MHz whip antenna was employed as the gateway. The sensor node, on the other hand, comprises the developed epidermal antenna connected to the wireless module using a U.FL-to-U.FL cable. Both the antenna and the module were mounted on the arm of a 34 year old male test subject weighing 70 kg and measuring 169 cm in height [see Fig. 14(b)]. The antenna was attached on the top side of the forearm, whereas the module was attached on the other side of the forearm. This configuration is in accordance with the simulations and measurements setups using the SPEAG arm phantom shown in Fig. 10. Inside the wireless module, there is also a temperature sensor. Biocompatible skin adhesives (LOCTITE DURO-TAK 222 from Henkel) were used for the attachment of the antenna and the module to the skin. The adhesives are very thin (i.e., 45 μm) and thus have an insignificant impact on the antenna performance as verified through simulations.

The LoRa module in the node was programmed to broadcast 10 packets containing the measured temperature and received signal strength indicator (RSSI) data to the gateways. As the temperature sensor is located on the circuit board, which is not in direct contact with the skin, we refer to the measured data as the ambient temperature near the test subject's arm. These packets were transmitted with a 10-s interval between each packet and an adaptive spreading factor (SF) setting between 7 to 12. The gateway was connected to the things network's (TTN) LoRaWAN network server, which was responsible for network and data management, such as performing security checks and adaptive data rate changes, filtering redundant received packets, and forwarding data packets to the user data portal for visualization and storage.

The test subject was subsequently instructed to move to five different locations labeled as A to E in Fig. 13. At each location, RSSI values from the three gateways were recorded for two distinct scenarios: 1) test subject standing with both arms at the side of the body [Fig. 14(c)] and 2) test subject standing with both arms raised [Fig. 14(d)]. Also calculated was the average of the RSSI values acquired from the same gateway. For comparison, the nontransparent antenna prototype was also subjected to this procedure. Out of the three average RSSI values obtained at each location, the maximum RSSI value, which was typically from the gateway nearest to the node and had PDR $= 1$, was noted. The results are presented in Fig. 15(a) and (b) for scenarios (1) and (2), respectively. The average ambient temperature measurements for each location are also shown. The results displayed in blue text (top line) pertain to the transparent prototype, whereas those displayed in green text (bottom line) correspond to the nontransparent prototype.

RSSI metric is a relative measurement of RF power level (in dBm) that in this case displays how effectively the gateway can receive the signal from the wirelessly connected sensor node. Notably, a LoRaWAN network can offer a maximum receiver sensitivity of -137 dBm at SF12 [45]. From the results, it is validated that the developed transparent epidermal antenna is capable of enabling the wireless functionality of the developed module. Despite the lossy operating environment, the antenna successfully establishes a communication link with at least one gateway in each of the predefined locations for both test cases. Following the trend shown in the far-field tests results, generally there is no substantial difference in the wireless link quality provided by the transparent and nontransparent prototypes.

D. SAR Numerical Analysis

The RF exposure of the antenna on the target human body part was evaluated numerically through calculated SAR distribution in CST Microwave Studio 2020. For this purpose, the antenna was mounted on the human forearm phantom shown in Fig. 2. The SAR distribution at 868 MHz was computed for an input power of 30 mW (maximum RF power supplied from the wireless module) and averaged over 10 g of tissue. As shown in Fig. 16, in terms of RF exposure, both the transparent and nontransparent epidermal antennas conform with the IEEE C95.1-2019 safety guideline for body extremities (i.e., SAR $<$ 4 W/kg) [46] for the specified maximum input power, frequency, and position on the body. The quality of the antenna conductor seems to have little impact on the RF exposure of an antenna in direct contact with human body tissue. The transparent antenna exhibits only a marginally lower SAR peak value (i.e., 0.688 W/kg) than its nontransparent

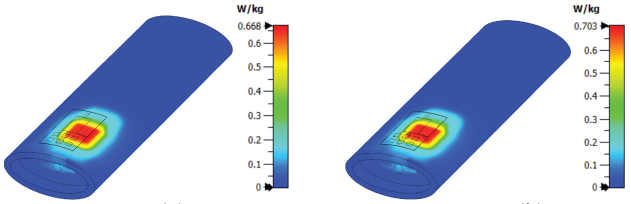

Fig. 16. Computed 10-g averaged SAR distributions at 868 MHz on forearm phantom: (a) transparent antenna and (b) nontransparent antenna.

counterpart (i.e., 0.703 W/kg), which may indicate slightly less power deposition on the body due to the lower textile conductivity. Nevertheless, this tiny less power loss on the body is compensated by a higher metal loss, resulting in the insignificantly lower radiated power observed in the results of the far-field tests.

VI. Conclusion

The common engineering strategy for achieving high comfort-of-wear in antennas for epidermal electronics is to impart skin conformability, which includes flexibility, stretchability, air/water permeability, biocompatibility, and ultrathinness. To complete the above qualities toward a truly unobtrusive epidermal antenna, we have successfully demonstrated the concept of optical transparency achieved through a simple and cost-effective layer-by-layer PDMS-textile assembly technique. Proof-of-concept arm-worn modified rectangular loop antennas (transparent and nontransparent prototypes) demonstrating good agreement between measurements and simulations were used to validate the idea. The findings reveal that due to the major power loss to the human body, the transparent epidermal antenna performs similarly to the nontransparent counterpart, despite the substantial difference in the quality of the conductive material. This suggests that one can increase the comfort-of-wear level of epidermal electronics by employing a transparent epidermal antenna without worrying about a major decline in wireless performance. A unique approach needs to be taken though when designing an epidermal antenna due to its strong interaction with the lossy human body. In the case of a modified loop antenna as presented in this study, the radiation performance can be controlled by the thickness of the underlying membrane, with conformability as a tradeoff, and the loop aperture. For the latter, one should aim for the optimal aperture size, which is the point of equilibrium between the opposing mechanisms of radiation and loss. This is in contrary to the free space case, in which a larger aperture always results in better radiation. Once the aforementioned parameters have been established, the width of the loop strip and its expanded side can be tuned to tailor the input impedance while preserving the radiation performance.

Acknowledgment

The authors would like to thank Professor Gaetano Marrocco of the University of Rome Tor Vergata for his invaluable feedback during the preparation of this manuscript, as well as Henkel, particularly Dr. Carla Negele, for providing samples of LOCTITE DURO-TAK 222.

References

[1] D.-H. Kim et al., "Epidermal electronics," *Science*, vol. 333, no. 6044, pp. 838–843, 2011.
[2] H. U. Chung et al., "Binodal, wireless epidermal electronic systems with in-sensor analytics for neonatal intensive care," *Science*, vol. 363, no. 6430, p. eaau0780, 2019.
[3] R. Herbert, J.-H. Kim, Y. S. Kim, H. M. Lee, and W.-H. Yeo, "Soft material-enabled, flexible hybrid electronics for medicine, healthcare, and human-machine interfaces," *Materials*, vol. 11, no. 2, p. 187, 2018.
[4] X. Huang et al., "Epidermal radio frequency electronics for wireless power transfer," *Microsyst. Nanoeng.*, vol. 2, no. 1, 2016, Art. no. 16052.
[5] H. A. Damis, N. Khalid, R. Mirzavand, H.-J. Chung, and P. Mousavi, "Investigation of epidermal loop antennas for biotelemetry IoT applications," *IEEE Access*, vol. 6, pp. 15806–15815, 2018.
[6] S. Amendola and G. Marrocco, "Optimal performance of epidermal antennas for UHF radio frequency identification and sensing," *IEEE Trans. Antennas Propag.*, vol. 65, no. 2, pp. 473–481, Feb. 2017.
[7] J. Kim, A. S. Campbell, B. E.-F. de Ávila, and J. Wang, "Wearable biosensors for healthcare monitoring," *Nat. Biotech.*, vol. 37, no. 4, pp. 389–406, 2019.
[8] L. Yin, K. N. Kim, A. Trifonov, T. Podhajny, and J. Wang, "Designing wearable microgrids: Towards autonomous sustainable on-body energy management," *Energy Environ. Sci.*, vol. 15, no. 1, pp. 82–101, 2022.
[9] D. P. Rose et al., "Adhesive RFID sensor patch for monitoring of sweat electrolytes," *IEEE Trans. Biomed. Eng.*, vol. 62, no. 6, pp. 1457–1465, Jun. 2015.
[10] J. Kim et al., "Epidermal electronics with advanced capabilities in near-field communication," *Small*, vol. 11, no. 8, pp. 906–912, 2015.
[11] S. Amendola, A. Palombi, and G. Marrocco, "Inkjet printing of epidermal RFID antennas by self-sintering conductive ink," *IEEE Trans. Microw. Theory Techn.*, vol. 66, no. 3, pp. 1561–1569, Mar. 2018.
[12] P. S. Taylor and J. C. Batchelor, "Finger-worn UHF far-field RFID tag antenna," *IEEE Antennas Wireless Propag. Lett.*, vol. 18, pp. 2513–2517, 2019.
[13] C. Miozzi, G. Stendardo, G. M. Bianco, F. Montecchia, and G. Marrocco, "Dual-chip RFID on-skin tag for bilateral breath monitoring," in *Proc. IEEE Int. Conf. RFID*, 2021, pp. 1–6.
[14] C. Occhiuzzi, S. Parrella, F. Camera, S. Nappi, and G. Marrocco, "RFID-based dual-chip epidermal sensing platform for human skin monitoring," *IEEE Sensors J.*, vol. 21, no. 4, pp. 5359–5367, Feb. 2021.
[15] F. Naccarata, G. M. Bianco, and G. Marrocco, "Sensing performance of multi-channel RFID-based finger augmentation devices for tactile Internet," *IEEE J. Radio Freq. Identif.*, vol. 6, pp. 209–217, 2022.
[16] M. Frattaioli, G. M. Bianco, S. Nappi, and G. Marrocco, "A finger-worn epidermal antenna for pressure sensing," in *Proc. 16th Eur. Conf. Antennas Propag. (EuCAP)*, 2022, pp. 1–4.
[17] N. Panunzio, E. Fontana, F. Montecchia, and G. Marrocco, "Two-channel epidermal RFID sensor for the wireless bilateral analysis of nasal respiration," *IEEE Sensors J.*, vol. 22, no. 23, pp. 23445–23455, Dec. 2022.
[18] J. D. Hughes, R. Horne, N. Brabon, and J. C. Batchelor, "An on-body UHF RFID tag with DDRR antenna for healthcare data streaming applications," *IEEE J. Radio Freq. Identif.*, vol. 6, pp. 680–687, 2022.
[19] M. C. Caccami, M. P. Hogan, M. Alfredsson, G. Marrocco, and J. C. Batchelor, "A tightly integrated multilayer battery antenna for RFID epidermal applications," *IEEE Trans. Antennas Propag.*, vol. 66, no. 2, pp. 609–617, Feb. 2018.
[20] D. O. Oyeka and J. C. Batchelor, "Robustness evaluation of an inkjet-printed epidermal ultra-high-frequency radio frequency identification tag," *Healthc. Techn. Lett.*, vol. 8, no. 1, pp. 18–23, 2021.
[21] J. D. Hughes, C. Occhiuzzi, J. Batchelor, and G. Marrocco, "Twin-grid array as 3.6 GHz epidermal antenna for potential backscattering 5G communication," *IEEE Antennas Wireless Propag. Lett.*, vol. 19, pp. 2092–2096, 2020.
[22] A. B. Barba, G. M. Bianco, L. Fiore, F. Arduini, G. Marrocco, and C. Occhiuzzi, "Design and manufacture of flexible epidermal NFC device for electrochemical sensing of sweat," in *Proc. IEEE Int. Conf. Flexible Printable Sens. Syst. (FLEPS)*, 2022, pp. 1–4.
[23] M. S. Rohei, E. Salwana, N. B. A. K. Shah, and A. S. Kakar, "Design and testing of an epidermal RFID mechanism in a smart indoor human tracking system," *IEEE Sensors J.*, vol. 21, no. 4, pp. 5476–5486, Feb. 2021.

[24] T. Shimura, S. Sato, P. Zalar, and N. Matsuhisa, "Engineering the comfort-of-wear for next generation wearables," *Adv. Elect. Mat.*, to be published.

[25] M. F. Farooqui and A. Shamim, "Low cost inkjet printed smart bandage for wireless monitoring of chronic wounds," *Sci. Rep.*, vol. 6, Jun. 2016, Art. no. 28949.

[26] M. Sheikh, M. Qassem, and P. A. Kyriacou, "Wearable, environmental, and smartphone-based passive sensing for mental health monitoring," *Front. Digit. Health*, vol. 3, Apr. 2021, Art. no. 662811.

[27] Z. Huang et al., "Recent advances in skin-like wearable sensors: Sensor design, health monitoring, and intelligent auxiliary," *Sens. Diagnos.*, vol. 1, pp. 686–708, Jun. 2022.

[28] C. Miozzi, F. Amato, and G. Marrocco, "Performance and durability of thread antennas as stretchable epidermal UHF RFID tags," *IEEE J. Radio Freq. Identif.*, vol. 4, pp. 398–405, 2020.

[29] A. S. M. Sayem, A. Lalbakhsh, K. P. Esselle, J. L. Buckley, B. O'Flynn, and R. B. V. B. Simorangkir, "Flexible transparent antennas: Advancements, challenges, and prospects," *IEEE Open J. Antennas Propag.*, vol. 3, pp. 1109–1133, 2022.

[30] A. S. M. Sayem, R. B. V. B. Simorangkir, K. P. Esselle, and R. M. Hashmi, "Development of robust transparent conformal antennas based on conductive mesh-polymer composite for unobtrusive wearable applications," *IEEE Trans. Antennas Propag.*, vol. 67, no. 12, pp. 7216–7224, Dec. 2019.

[31] R. B. V. B. Simorangkir, Y. Yang, R. M. Hashmi, T. Björninen, K. P. Esselle, and L. Ukkonen, "Polydimethylsiloxane-embedded conductive fabric: Characterization and application for realization of robust passive and active flexible wearable antennas," *IEEE Access*, vol. 6, pp. 48102–48112, 2018.

[32] M. G. Ahlström, J. P. Thyssen, M. Wennervaldt, T. Menné, and J. D. Johansen, "Nickel allergy and allergic contact dermatitis: A clinical review of immunology, epidemiology, exposure, and treatment," *Contact Dermatitis*, vol. 81, no. 4, pp. 227–241, 2019.

[33] J. DeMarinis, "The antenna cable as a source of error in EMI measurements," in *Proc. IEEE Int. Symp. Electromagn. Compat.*, 1988, pp. 9–14.

[34] O. Staub, J.-F. Zürcher, and A. Skrivervik, "Some considerations on the correct measurement of the gain and bandwidth of electrically small antennas," *Microw. Opt. Technol. Lett.*, vol. 17, no. 3, pp. 156–160, 1998.

[35] D. R. Gawade et al., "A museum artefact monitoring testbed using LoRaWAN," in *Proc. IEEE Symp. Comput. Commun. (ISCC)*, 2021, pp. 1–3.

[36] A. Abbosh, "Accurate effective permittivity calculation of printed Center-fed dipoles and its application to quasi Yagi–Uda antennas," *IEEE Trans. Antennas Propag.*, vol. 61, no. 4, pp. 2297–2300, Apr. 2013.

[37] "SPEAG OTA phantom, SHO generic forearm phantom CTIA version 1." Accessed: Feb. 15, 2021. [Online]. Available: https://speag.swiss/products/em-phantoms/ctia-sub-3/sho-gfpc-v1/

[38] *Test Plan for Wireless Device Over-the-Air Performance: Method of Measurement for Radiated RF Power and Receiver Performance, Version 3.9.5*, CTIA Certification, Washington, DC, USA, Sep. 2022.

[39] C. Gabriel, "Tissue equivalent material for hand phantoms," *Phys. Med. Biol.*, vol. 52, no. 14, pp. 4205–4210, 2007.

[40] S. Gabriel, R. W. Lau, and C. Gabriel, "The dielectric properties of biological tissues: II. Measurements in the frequency range 10 Hz to 20 GHz," *Phys. Med. Biol.*, vol. 41, no. 11, pp. 2251–2269, 1996.

[41] C. Gabriel, "Comments on 'dielectric properties of the skin"' *Phys. Med. Biol.*, vol. 42, no. 8, pp. 1671–1674, 1997.

[42] S. Saario, D. V. Thiel, J. W. Lu, and S. G. O'Keefe, "An assessment of cable radiation effects on mobile communications antenna measurements," in *IEEE Antennas Propag. Soc. Int. Symp. Dig.*, vol. 1, 1997, pp. 550–553.

[43] A. S. M. Sayem et al., "Flexible and transparent circularly polarized patch antenna for reliable unobtrusive wearable wireless communications," *Sensors*, vol. 22, no. 3, p. 1276, 2022.

[44] "The things gateway." Accessed: Jul. 13, 2021. [Online]. Available: http://www.farnell.com/datasheets/2552236.pdf

[45] "Understanding the LoRa adaptive data rate," Semtech Corp., Camarillo, CA, USA, Rep., 2019, pp. 1–15. [Online]. Available: https://lora-developers.semtech.com/library/tech-papers-and-guides/understanding-adr/

[46] *IEEE Standard for Safety Levels With Respect to Human Exposure to Electric, Magnetic, and Electromagnetic Fields, 0 Hz to 300 GHz*, IEEE Standard C95.1-2019, 2019.

Roy B. V. B. Simorangkir (Member, IEEE) received the B.S. degree in telecommunication engineering from Bandung Institute of Technology, Bandung, Indonesia, in 2010, the M.S. degree in electrical and electronic engineering from Yonsei University, Seoul, South Korea, in 2014, and the Ph.D. degree in electronic engineering from Macquarie University, Sydney, Australia, in 2018.

He is currently with the Wireless Sensor Network group, Tyndall National Institute, Cork, Ireland, as a Senior Postdoctoral Researcher. His general research interest is the development of unconventional materials-based antennas and sensors for next generation wireless communication and sensing systems. He has over 60 referred publications in this area.

Dr. Simorangkir was a recipient of a number of major awards. He was awarded the Highly Competitive Korean Government Scholarship Program from 2012 to 2014 for his master's degree. During his Ph.D., he succeeded the International Macquarie University Research Excellence Scholarship from 2015 to 2018, the Macquarie University Postgraduate Research Fund with the Deputy Vice-Chancellor Commendation in 2017, and the Wireless Medical Research Centre Travel and Project Grants from 2015 to 2017. In 2017, he was a part of the team who won the Macquarie Student Startup Pitch Competition and the Commonwealth Scientific and Industrial Research Organisation sponsored ON PRIME 2 Preaccelerator Fund for research commercialization. In the same year, one of his works received the first prize in the IEEE Region 10 (Asia–Pacific) Best Student Paper Contest (Postgraduate Category) and was a finalist in the Student Paper and Advanced Practice Paper Competitions of the IEEE MTT-S International Microwave Symposium, Honolulu. He was recently granted the prestigious 2022 Government of Ireland Fellowship to further his research on fully printed multimode adaptive antennas. He is currently serving as a Guest Editor of Special Issues of Sensors and Electronics. He was the Special Session Co-Chair in the 2018 International Applied Computational Electromagnetics Society Symposium, Beijing, the 2021 Asia–Pacific Microwave Conference (APMC), Adelaide, and the 2021 IEEE International Symposium on Antennas and Propagation, Singapore. He served as the Publicity Chair of the 2022 International Workshop on Antenna Technology, Dublin. He has been a frequent reviewer for several reputable journals in his research field. He was acknowledged as an Outstanding Reviewer of the IEEE TRANSACTION ON ANTENNAS AND PROPAGATION for two consecutive years, 2021 and 2022, respectively.

Dinesh R. Gawade (Member, IEEE) received the Bachelor of Technology degree in electronics and communication technology from the Department of Technology, Shivaji University, Kolhapur, India, in 2016. and the M.Eng.Sc. degree from Tyndall National Institute, University College Cork, Cork, Ireland, in 2022. He is currently pursuing the Ph.D. degree with Tyndall National Institute and Microelectronic Circuit Center Ireland, Cork.

Following his graduation, he gained valuable industry experience as a Hardware Design Engineer from 2016 to 2018. Subsequently, he contributed his expertise to the Indian Institute of Technology Mandi, Mandi, India, as a Project Engineer specializing in Hardware Design. In 2019, he joined Tyndall National Institute, University College Cork, to further advance his research and career. His research interests encompass a broad range of topics, including the development of batteryless sensing devices, radio-frequency integrated circuit design, antenna design, low-power sensor node design, and design of long-range wireless sensor network for various application.

Tim Hannon (Member, IEEE) received the M.Eng. degree from ITT-Dublin, Dublin, Ireland, in 2004, and the B.Eng. degree in electronic engineering from the University College Dublin, Dublin, Ireland, in 2002.

He has 20 years of design experience in multiple sectors and industries, including Hardware Design, RF Design, Embedded Software Development, Cloud Software Development, IOT Technologies, and Data Analytics. He is currently working as a Researcher in residence with Tyndall National Institute, Cork, Ireland, for Sanmina Corporation, Huntsville, AL, USA, collaborating with both industrial and academic partners with principal focus on research and design of connected wearable healthcare sensors. He previously worked as Chief Technical Officer with HerdInsights, Cork, an Agri-Tech company, starting from the ground up with greenfield devices and progressing to volume production of internationally exported devices with scalable cloud infrastructure. His previous other roles mostly focussed on RF design in SME companies.

Paul Donovan (Member, IEEE) received the Bachelor of Electronic Engineering degree from the University of Limerick, Limerick, Ireland, in 1987, and the Post Graduate Diploma degree in hierarchical electronic design from the University of Delft, Delft, Netherlands, in 1989.

He is a Senior R&D Program Manager for wearable medical device research with Sanmina, San Jose, California. He joined Philips BV Netherlands as an Analog IC designer leading design of digital audio DAC IC products. He joined as an Intel Corporation Test Development Engineering and held multiple design, test, and product wafer fabrication operations Senior Leadership roles. He established a Product Development Team with responsibility for VLSI scan test design. His current research interests include the design, prototype manufacture, and clinical investigation of smart wearable devices for medical and well-being diagnostics with applications in sepsis screening and multiple biomarker monitoring. His focus is on collaborative system design integration of multiple technologies to create novel wearable medical device prototypes suitable for clinical investigation.

Dr. Donovan received an Intel Award in 2002 for rearchitecting Intel's NPI system. He was a Founding Member of Intel Custom Foundry Business Unit with ownership of design to silicon systems including Intel Multi-Product Shuttle Silicon Design Prototyping Operation. He was previously a Committee Member of MIDAS Ireland and an IEI Member.

Sanjeev Kumar (Member, IEEE) received the B.Tech. degree in electronics and communications engineering from Sam Higginbottom University of Agriculture, Technology and Sciences, Prayagraj, India, in 2012, the M.S. by Research degree in electronics and communications engineering from The LNM Institute of Information Technology, Jaipur, India, in 2015, and the Ph.D. degree in electrical and electronic engineering from the University College Cork, Cork, Ireland, in 2021.

From 2012 to 2013, he worked as a Telecom Engineer with Wipro, Mumbai, India. From 2015 to 2016, he held the position of an Assistant Professor with the Department of Electronics and Communication Engineering, Pratap Institute of Technology and Science, Sikar, India. Since February 2022, he has been a Postdoctoral Researcher with the Wireless Sensor Networks Group, Tyndall National Institute, University College Cork. His research interests include the design and development of electrically small antennas, wearable and implantable antennas, NFC and RFID, bandwidth enhancement techniques, circuit modeling, and embedded hardware design.

Dr. Kumar was a recipient of the LNMIIT Merit-Based Scholarship during his master's studies, and his Ph.D. research was supported through grants from Enterprise Ireland and Science Foundation Ireland Connect Centre.

Nadeem Rather (Student Member, IEEE) received the bachelor's degree in engineering, specializing in electronics and communication, and the master's degree in Engineering, with a focus on communication systems. He is currently pursuing the Doctoral Research degree with the Wireless Sensor Networks Group, Tyndall National Institute, University College Cork, Cork, Ireland.

His research focuses on developing advanced AI algorithms and innovative techniques for enhancing the performance and efficiency of RFID systems. His research also encompasses the design of RF antennas tailored for wearable health monitoring applications. Additionally, he possesses extensive industry and research experience, enriching his expertise in the field.

Throughout his doctoral journey, Dr. Nadeem's contributions have been recognized through notable accolades. He was honored with the Postgraduate Publication of the Year 2020 Award at Tyndall National Institute. Furthermore, his research paper secured the first place in the Best Student Research Paper Category at the International Workshop on Antenna Technology 2021. Additionally, his research work was acknowledged with the Best Demonstration Award at the VistaMilk Conference 2023, highlighting the practical impact of his innovative solutions. In addition to his research endeavors, he plays a vital role as a Vice Chair of the Tyndall Early Career Researchers Network, affiliated with the Young European Associated Researchers Network. In this capacity, he passionately promotes collaboration and knowledge exchange among fellow researchers, actively contributing to the growth and advancement of the scientific community.

Gholamhosein Moloudian (Member, IEEE) received the Associate's degree (Highest GPA, first-class Hons.) in electronic and electrical engineering from Technical and Vocational University, Yasouj, Iran, in 2008, and the B.Sc. degree in electronic and electrical engineering from the Higher Education Center, Shiraz, Iran, in 2010, and the M.Sc. degree (Highest GPA, first-class Hons.) in electronic and electrical engineering from Islamic Azad University (IAU) of Bushehr, Bushehr, Iran, in 2012, and the Ph.D. degree (Hons.) in electronic and electrical engineering from IAU, Arak Branch, Arak, Iran, in 2018.

He worked as a Researcher and a Lecturer with the Department of Electrical Engineering, Salman Farsi University of Kazerun, Kazerun, Iran, and IAU of Kazerun, Kazerun, Iran, from January 2016 to September 2020. Moreover, He worked with the South Electrical Management Company in the field of industrial sensors and energy efficiency, from October 2020 to December 2021. He is currently working with the Wireless Sensor Networks Group (Antenna/RF Team), Tyndall National Institute, University College Cork, Cork, Ireland, as a Marie Skłodowska-Curie Research Fellow and a SMART 4.0 Fellow (with the SFI-CONFIRM Center). His research interests include design and analysis of RF/microwave circuits, energy harvesting, RF low-power electronic circuits, PCB design, RFID, microstrip antennas and sensors, and 2-D photonic devices.

Brendan O'Flynn (Senior Member, IEEE) received the B.Eng. (Hons.), M.Eng.Sc., and Ph.D. degrees from the University College Cork, Cork, Ireland, in 1993, 1995, and 2016, respectively.

He is currently a Senior Staff Researcher with the Tyndall National Institute, Cork, where he is also the Head of the Wireless Sensor Networks Group. His research interests include wearable sensing systems, edge-based analytics, sensor system integration, low-power embedded systems design and development, system miniaturization, and RF system design and optimization. He has published widely in these areas and has secured significant funding for the development and deployment of "Smart Sensing" technologies and applied research projects.

John L. Buckley (Member, IEEE) was born in Cork, Ireland. He received the B.Eng. degree from the Cork Institute of Technology, Cork, in 1994, and the M.Eng.Sc. and Ph.D. degrees from the Department of Electrical and Electronic Engineering, University College Cork, Cork, in 2004 and 2016, respectively.

From 1994 to 2002, he was with EMC Corporation, Cork, where he specialized in PCB design, High-Speed Digital Design and Signal Integrity. He joined the Tyndall National Institute, University College Cork, in 2005, where he is currently a Senior Researcher and leads the Antenna and RF Team's research activities working on both fundamental and applied antenna and RF research. He has published more than 80 scientific works and acts as a reviewer for several international antenna journals and conferences in the field of Antennas and Propagation. His research interests include electrically small antenna design, tunable antennas, wearable and implantable antennas, and RF front-end design.

Dr. Buckley served as a General Co-Chair for the International Conference on Antenna Technology in 2022.